arXiv:2506.10605v3 [cs.CV] 5 Sep 2025

High-resolution efficient image generation from WiFi CSI using a pretrained latent diffusion model

Eshan Ramesh, Takayuki Nishio
School of Engineering, Institute of Science Tokyo
Email: esrh@esrh.me, nishio@ict.eng.isct.ac.jp

***Abstract*—We present LatentCSI, a novel method for generating images of the physical environment from WiFi CSI measurements that leverages a pretrained latent diffusion model (LDM). Unlike prior approaches that rely on complex and computationally intensive techniques such as GANs, our method employs a lightweight neural network to map CSI amplitudes directly into the latent space of an LDM. We then apply the LDM's denoising diffusion model to the latent representation with text-based guidance before decoding using the LDM's pretrained decoder to obtain a high-resolution image. This design bypasses the challenges of pixel-space image generation and avoids the explicit image encoding stage typically required in conventional image-to-image pipelines, enabling efficient and high-quality image synthesis. We validate our approach on two datasets: a wide-band CSI dataset we collected with off-the-shelf WiFi devices and cameras; and a subset of the publicly available MM-Fi dataset. The results demonstrate that LatentCSI outperforms baselines of comparable complexity trained directly on ground-truth images in both computational efficiency and perceptual quality, while additionally providing practical advantages through its unique capacity for text-guided controllability.**

I. Introduction

WiFi channel state information is typically computed in the process of equalizing received symbols using known sync words and pilot carriers. However, especially in multi-carrier systems, it contains rich information about the propagation environment. The ubiquity of WiFi therefore makes CSI an attractive source of data for sensing applications. Data-driven methods for recovering physical information from the CSI of a multi-carrier wireless link are well studied. With the power of machine learning techniques, researchers have succeeded in accomplishing a wide variety of sensing tasks, including pose estimation and activity classification [1], and with sufficient bandwidth, even as finely-grained tasks as sensing human breathing at a distance. While existing research has confirmed the feasibility, and indeed the surprising practicality, of using CSI to predict low-dimensional indicators of the physical world, work showing high-dimensional environment reconstruction capability is comparatively scarce.

In this work, we are interested in generating high resolution RGB camera images from CSI. In the human sensing case (which is a primary focus of the CSI sensing domain) camera images effectively superset the information gained from pose estimation and activity classification. Image generation is considerably more complex, demanding good perceptual structure and high output dimensionality.

Given these challenges, many prior works have adopted generative adversarial networks (GANs) [2] as a solution for CSI-based image generation. The GAN framework trains two models against each other: a generator that learns the target distribution and a discriminator that learns to distinguish generated samples from real samples. GAN-based approaches were some of the first to be applied to generating images from CSI; one of the first direct CSI to image works [3] developed a GAN to generate a 64x64 RGB image. The authors demonstrated their method correctly classifying objects and positioning human subjects, but they noted poor performance on humans in motion. Subsequent work in [4] and [5] applies the GAN framework to transform images using information determined from CSI using pose keypoints determined from CSI, which circumvents the challenge of generating images from scratch. While GANs have shown promise, they introduce significant complexity into the training process, as they require training two models simultaneously and careful tuning to ensure stability and convergence [6]. This complexity motivates the exploration of simpler models with more straightforward training procedures. A recent non-GAN approach addressing this issue is presented in [7], where the authors propose a mixture-of-product-of-experts variational autoencoder (VAE) that jointly trains an MLP-based CSI encoder and a ground-truth image encoder.

Despite these efforts, the existing literature remains limited in image resolution and computational efficiency. Moreover, to our knowledge, the existing methods—including both GAN-based and non-GAN approaches—rely on end-to-end training with ground-truth images. As a result, the model tends to fit the image data very well, leading to generated outputs that inadvertently reproduce fine visual features. This is particularly concerning in privacy-sensitive scenarios, where unintended reconstruction of details such as facial features may pose significant privacy risks.

To address these limitations, we propose LatentCSI, a novel image generation scheme that leverages a pretrained latent diffusion model (LDM). Diffusion models have recently gained attention for their ability to produce high-quality images through iterative denoising guided by text embeddings. Latent diffusion models in particular operate in a lower-dimensional latent space rather than the color pixel space, enabling faster

This work was supported by JSPS KAKENHI Grant Number 23K24831 and 23K26109, and JST ASPIRE Grant Number JPMJAP2346, Japan. Models were trained on the TSUBAME4 supercomputer at the Institute of Science Tokyo.

and more memory-efficient image synthesis.

Compared to existing methods, LatentCSI adopts a simpler design that trains a single, lightweight neural network to predict latent embeddings directly from CSI data. The reduced dimensionality of the output, combined with the expressive power of a pretrained LDM diffusion model and decoder allows for the generation of high-resolution images at a lower computational cost. Moreover, since the LDM supports text-guided image generation, our approach naturally enables an optional refinement step, in which the generated image can be modified according to textual instructions—for example, altering a person's face or clothing appearance to match a given description. Importantly, the low-dimensional bottleneck in our encoding-decoding pipeline inherently reduces the risk of reproducing sensitive fine-grained details such as facial features, clothing, or background elements. At the same time, the LDM can synthesize visually plausible content aligned with user intent via text-guided modification, striking a balance between interpretability and privacy. This capability enables controllable and privacy-preserving image generation while preserving a meaningful correspondence with the underlying CSI signals.

The primary contribution of this work is the introduction of an LDM-based framework for generating images of the physical environment from CSI data. Our approach achieves state-of-the-art resolution and text-conditioned image synthesis with a simple architecture, a straightforward training procedure, and low computational overhead. We validate our method using two paired CSI–image datasets: one collected through experiments involving variations in a walking subject's position and orientation; and another based on a subset of the publicly available MM-Fi dataset [8], selected to represent diverse human poses with less visual complexity. For both datasets, we qualitatively evaluate the generated images and quantitatively compare our approach against a baseline model trained end-to-end on full-resolution images and the hybrid GAN strategy introduced in CSI2Image [3].

II. Methodology

A. System model

We consider a WiFi sensing system designed to monitor indoor environments by capturing human activity through wireless signals. The system consists of a WiFi access point, a WiFi terminal, and an RGB camera that is available only during the training phase. This setup enables the collection of paired channel state information (CSI) and image data, which are used to train an image generation model. LatentCSI, is intended for practical scenarios in which camera imagery can be collected temporarily—such as during initial system calibration—but becomes unavailable during deployment due to obstructions or privacy concerns. As a result, while the model leverages visual data during training, inference is performed exclusively using CSI, making the approach suitable for privacy-sensitive or camera-limited environments.

For the approach to be feasible, it is essential that the CSI measurements carry sufficient information to represent the perceptual variations present in the visual scene. This requires a strong correspondence between fluctuations in CSI and changes in image content—i.e., sufficient mutual information between the two modalities. This assumption, while often implicit, is fundamental to all prior work on CSI-based image generation. If the perceptual alignment or the expressive capacity of CSI is lacking, learning a reliable mapping from CSI to visual content becomes fundamentally difficult.

Finally, we assume access to a publicly available pretrained latent diffusion model, such as Stable Diffusion, which provides a complete pipeline composed of an encoder for mapping RGB images into a latent space, a decoder for reconstructing images from latent representations, and a denoising diffusion model for generating and refining latent representations. The availability and perceptual quality of this fully pretrained LDM is essential to our approach, as it enables high-quality image synthesis in a computationally efficient manner, eliminating the need to train large generative models from scratch.

B. Overview of LatentCSI

Our proposed method, LatentCSI, builds upon a pretrained latent diffusion model, Stable Diffusion v1.5 [9]. To clarify our design, we first describe the standard inference process of LDMs. We proceed to introduce our modified inference procedure, which adapts an image-to-image pipeline to use CSI instead of images. The training procedure of the key component in this pipeline—the CSI encoder that predicts the LDM's latent representation—is presented in the following section.

1) LDM image-to-image pipeline: Diffusion models generate images by reversing a diffusion process, progressively transforming sampled Gaussian noise into an image through iterative denoising guided by conditioning inputs such as text prompts. In contrast, the image-to-image procedure, popularized in [10], starts from an input image, adds noise to simulate forward diffusion up to a chosen intermediate timestep, and then denoises to produce the output.

Latent diffusion models perform denoising in latent space rather than pixel space, offering performance benefits. Since our implementation of LatentCSI is based on Stable Diffusion, we describe the LDM's operation according to the implementation of Stable Diffusion. While different implementations of LDM may vary in model architecture, their fundamental operation remains the same. The image-to-image pipeline of an LDM is illustrated in Figure 1.

A VAE with Kullback–Leibler (KL) regularization, trained on large datasets to preserve perceptual structure under compression, serves as the encoder and decoder to map between image and latent spaces. The denoising diffusion model, a U-Net, is trained to estimate and remove noise at each diffusion timestep, conditioned on text embeddings.

In the LDM image-to-image process, the input image is first encoded into a latent embedding, to which a parametrized amount of noise is added. This noisy latent embedding is then iteratively denoised by the denoising diffusion model, guided by conditioning inputs (e.g., a text prompt). Finally, the decoder maps the denoised latent embedding back to image space to generate the target image.

The variance of noise added to the latent vectors before they are passed through the denoising diffusion model, and therefore the intermediate timestep the reverse process begins at, is an important parameter, typically called “strength”. The closed-form expression for the noise variance depends on the diffusion algorithm and variance schedule used. Lower strength corresponds to output images that more closely resemble the input, and higher strength induces more significant transformations.

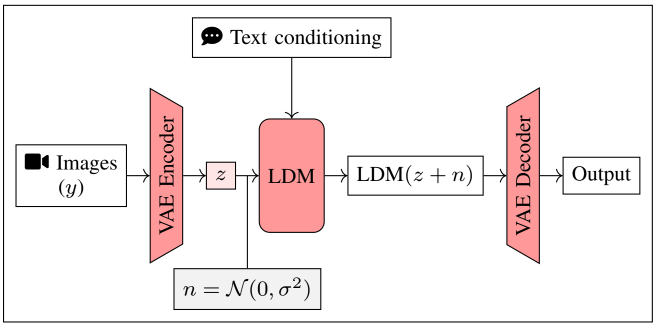

Fig. 1. Stable diffusion LDM img2img pipeline

2) LatentCSI Inference Process: Figure 2 shows the inference pipeline of LatentCSI. The key difference from the standard LDM pipeline is that the VAE encoder is replaced with a CSI encoder, enabling the LDM’s latent starting point to be estimated directly from CSI instead of an image. Similar to an LDM, data in the LatentCSI pipeline is processed primarily in latent space, in contrast to existing CSI-to-image generation methods that directly map CSI to image space. This latent-space design reduces computational cost, as the latent embedding has much lower dimensionality than high-resolution images.

The CSI encoder plays a crucial role by mapping CSI measurements into the latent space expected by the LDM’s denoising model. The accuracy of this latent embedding is vital, as it serves as the input for the subsequent denoising and decoding stages. Once the latent embedding is estimated by the CSI encoder, it is iteratively denoised by the pretrained denoising diffusion model under text-based conditioning, and finally decoded into an image using the pretrained decoder.

We emphasize that the only modified component in this otherwise standard LDM pipeline is the custom CSI encoder. As a result, training is straightforward and computationally light, since only the CSI encoder needs to be fitted while all other components can be used without finetuning. The training procedure for the CSI encoder is detailed in the following section.

C. LatentCSI training process

The CSI encoder is trained to map CSI measurements into the latent space of the LDM as a probabilistic model. Specifically, let x denote the CSI input and y the corresponding image. We model the behavior of the CSI encoder as a probabilistic distribution $p_w(z|x)$, parameterized by w, analogous to the pretrained VAE encoder $q_\Phi(z|y)$ of the LDM. The goal is to train $p_w(z|x)$ so that its output distribution closely matches $q_\Phi(z|y)$. This is achieved by minimizing the divergence between the latent samples from $p_w(z|x)$ and $q_\Phi(z|y)$ over paired training data. In other words, the CSI encoder learns to approximate the latent distribution produced by the pretrained VAE encoder for the corresponding image.

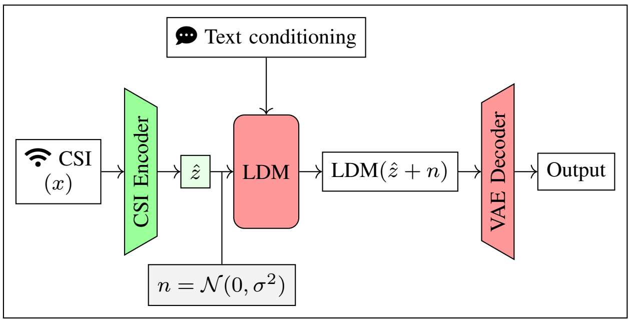

Fig. 2. LatentCSI: img2img with custom CSI encoder

The pretrained VAE encoder $q_\Phi(z|y)$ models the posterior latent distribution as a Gaussian with a diagonal covariance matrix:

$$q_\Phi(z|y) = \mathcal{N}(\mu_\Phi(y), \text{diag}(\sigma_\Phi^2(y)))$$

with $\mu_\Phi(y), \sigma_\Phi^2(y) \in \mathbb{R}^{4\times64\times64}$. To obtain a sample z, we draw from the distribution using the reparameterization trick: $z = \mu + \sigma \odot \epsilon, \quad \epsilon \sim \mathcal{N}(0, I)$. In the VAE of Stable Diffusion v1.5, the predicted variance $\sigma_\Phi^2(y)$ has been empirically observed to be very small, resulting in sampled latent vectors z concentrating closely around the mean. Therefore, we directly use $\mu_\Phi(y)$ as the latent embedding: $z := \mu_\Phi(y)$.

As a result of this choice, we redefine the CSI encoder as a deterministic neural network $f_w(x)$, which predicts the latent mean $\mu_\Phi(y)$ from a CSI measurement x, replacing the earlier probabilistic formulation. The detailed architecture of the CSI encoder is described in the following subsection. The CSI encoder is trained by minimizing the squared error between its output and the corresponding latent mean:

$$\min_w \mathbb{E}_{(x,y)\sim\mathcal{D}} \left[\| f_w(x) - \mu_\Phi(y) \|_2^2 \right].$$

Here, $\mathcal{D}$ denotes the empirical joint distribution of paired training samples (x, y), where x is a CSI measurement and y is the corresponding RGB image captured simultaneously during data collection.

The overall training procedure is illustrated in Figure 3. The CSI encoder learns to regress directly to the mean latent representation produced by the pretrained VAE encoder for each corresponding image y. In our approach, the CSI input x uses only amplitude information. Given a complex-valued CSI measurement $x_c \in \mathbb{C}^s$, the input is computed as $x = \sqrt{\text{Re}(x_c)^2 + \text{Im}(x_c)^2}$. This choice follows prior work [1] [4] [7] suggesting that amplitude alone is sufficient for many sensing tasks, and avoids the additional complexity of handling phases in unsynchronized device configurations.

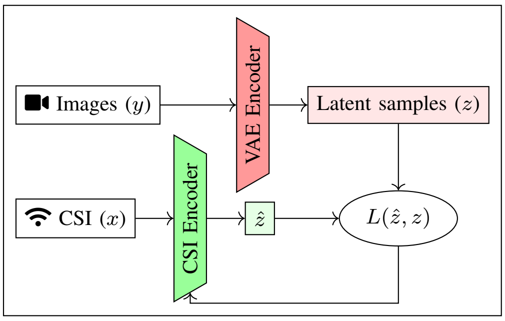

Fig. 3. CSI encoder training procedure

D. Model architecture

Our model architecture is shown in Figure 4. The input to the model is the preprocessed amplitude of the CSI signal, and the output is a latent embedding in the latent space of the pretrained VAE in the LDM pipeline.

We first apply a fully connected layer to map the 1D CSI input of size s to a 1D vector before reshaping it into a tensor with b channels, where b is a tunable parameter. We use 4 upsampling steps that each halves the number of channels and doubles the resolution. We then use a final convolutional layer to reduce the number of channels to the output specification. Each upsampling layer consists of two residual blocks and a transpose convolutional layer. Each residual block is itself composed of two convolutional layers. The last 3 upsampling steps use a cross attention layer to ensure that later spatially upsampling blocks attend to global information. This architecture strongly resembles that of the Stable Diffusion VAE encoder, which uses 4 similar downsampling steps followed by convolutional layers.

III. Evaluation

We evaluate LatentCSI on two datasets. For each dataset, we present a qualitative analysis using sample reference and generated images from the test sets withheld from the model.

To quantitatively assess the performance of the proposed method, we compare ground-truth images with predicted images without the application of latent diffusion transformations—specifically, the noising strength parameter in the inference pipeline is set to zero. This ensures that the output remains faithful to the direct predictions of the CSI encoder for an interpretable and unbiased evaluation.

We use three metrics in our analysis: the pixel-wise Root Mean Square Error (RMSE), the Structural Similarity Index Measure (SSIM), and the Fréchet Inception Distance (FID). RMSE and SSIM provide image-level comparisons and are sensitive to absolute and structural differences, respectively. In contrast, FID offers a perceptual measure of distributional similarity.

For both datasets, we report these metrics in two cases: (1) using the entire generated and reference images, and (2) using cropped image regions containing human figures, as identified by the YOLOv3 object detection model [11]. Given the human-centric nature of the datasets, the second case provides a focused evaluation of the model's ability to preserve semantically important content.

In both evaluation schemes, we benchmark LatentCSI against two strategies: a baseline model using the exact same architecture and training procedure as LatentCSI but predicting pixels directly; and the "hybrid" GAN strategy (K=8) from CSI2Image[3] which combines supervised loss with adversarial conditional GAN loss.

LatentCSI and the baseline model were trained using an early stopping criterion for validation loss stagnation over 5 consecutive training epochs. We used the ADAM optimizer with a fixed learning rate of 0.0005. To account for variability arising from stochastic weight initialization and training dynamics, each model was trained 5 times. Image samples are generated using the model instance with the best test loss. All experiments were conducted on a system equipped with a single NVIDIA H100 GPU and eight CPU cores of an AMD EPYC 9654 processor.

A. Dataset 1: Position & orientation of one moving human subject

We first evaluate the proposed method on a custom dataset designed to assess performance in predicting the position and orientation of a moving human subject. Data was collected from a single individual walking back and forth in a small indoor environment. CSI measurements were recorded at 10 Hz over 25 minutes using two ASUS NUCs equipped with Intel AX210 wireless cards, operating over a 160 MHz channel with a single transmit-receive antenna pair. A total of 1992 subcarriers were captured per sample using the FeitCSI tool [12]. Each CSI sample was paired with a synchronized 640×480 RGB image captured via an Intel Realsense D435 camera. The resulting 15,000 image-CSI pairs were post-processed by cropping and resampling images to 512×512 resolution. Facial features were blurred only in the presented examples; unaltered images were used for training and inference. The dataset was split into 80% training, 10% validation, and 10% testing. The CSI encoder model was configured with $b = 256$ initial channels, yielding 22,914,052 trainable parameters. The baseline model used $b = 8$ and comprised 16,434,395 parameters.

Table I presents representative samples from the test set, while quantitative results are shown in Table III. LatentCSI exhibits marginal improvements over the baseline in RMSE and SSIM, but achieves a substantially lower FID, indicating superior perceptual quality. This advantage is further amplified when evaluation is restricted to regions containing human figures, suggesting better reconstruction of salient information. Despite comparable model complexity, the baseline model—which directly predicts pixel values—requires approximately three times longer to train, owing to the increased output dimensionality. Dataset 1 presents a realistic, unsanitized setting with diverse views of a moving subject and

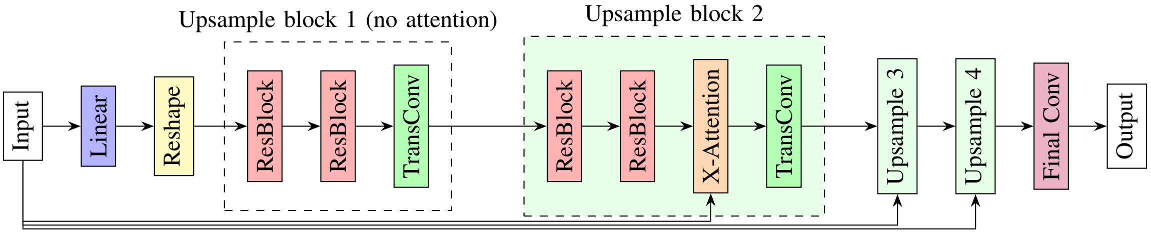

Fig. 4. Diagram of CSI encoder model

TABLE I
SAMPLE IMAGE COMPARISON FROM DATASET 1

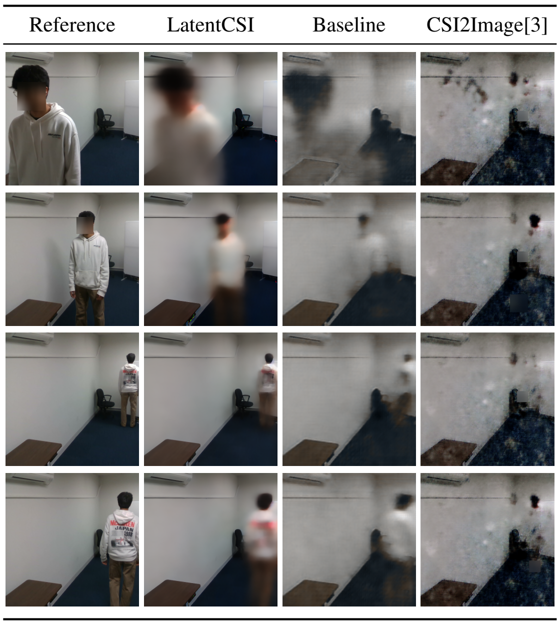

TABLE II
SAMPLE IMAGE COMPARISON FROM DATASET 2

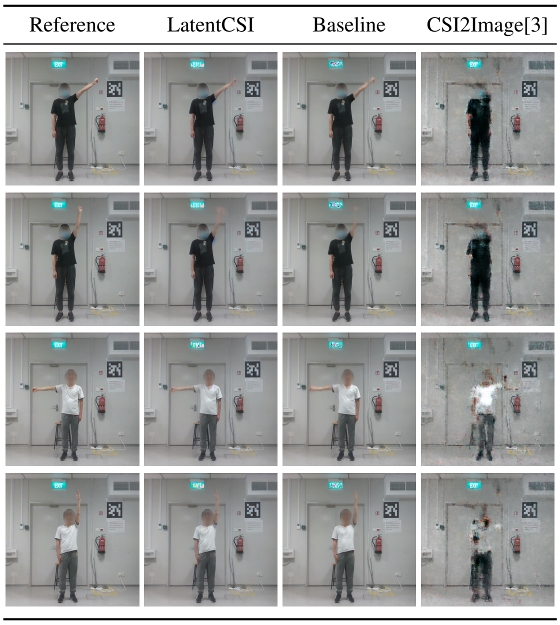

frequent occlusions. These factors increase pose significant challenges for pixel-space prediction.

Qualitative results indicate that the baseline and CSI2Image underfit the dataset, likely constrained by their limited capacity to model high-resolution pixel distributions. In contrast, LatentCSI produces better reconstructions with a smaller model. These outputs serve as effective initialization points for downstream diffusion-based refinement, as shown in Table IV.

B. Dataset 2: Human poses with MM-Fi

We evaluate our proposed method on the popular MM-Fi dataset [8]. Data is collected from 3 antennas each using 114-carrier 40 MHz channels, resulting in 342 total subcarriers. Compared to Dataset 1, this offers lower spectral resolution but greater spatial diversity. The selected subset comprises environment 3, the first two subjects, and four arm movement activities: 13–14 (raising hand, left/right) and 17–18 (waving hand, left/right), totaling 23,760 samples. The proposed model is configured with $b = 256$ and has 13,621,252 parameters; the baseline uses $b = 32$ with 11,490,275 parameters.

Table II and Table III present qualitative and quantitative results, respectively. Unlike Dataset 1, the visual consistency of MM-Fi—fixed subject position and minimal background variation—enables the baseline model to perform well, particularly in terms of RMSE and SSIM. This reflects its ability to memorize low-variance visual features through direct pixel supervision.

However, the proposed method outperforms the baseline in FID, indicating superior perceptual quality. When evaluation is restricted to regions containing human subjects, the RMSE and SSIM differences narrow, while the FID advantage of the proposed model approximately doubles. Qualitative analysis suggests the baseline model tends to produce artifacts and anatomically implausible outputs. The CSI2Image model is significantly underfit, and likely requires architecture tuning to work well with the higher resolution used in this work. In contrast, the latent-space model yields more coherent representations of salient features.

C. Text-guided CSI Image Generation

Our choice of latent space as that of the Stable Diffusion LDM enables text-guided manipulation of generated images without requiring an image encoding step. This capability allows us to refine or alter the visual content of CSI-generated

TABLE III
QUANTITATIVE COMPARISON OF METHODS OVER 5 RUNS

Method	FID ↓	RMSE ↓	SSIM ↑	FID (crop) ↓	RMSE (crop) ↓	SSIM (crop) ↑	Sec/epoch	Time (min:s)
Dataset 1 LatentCSI	**134.23 ± 7.18**	**18.95 ± 0.44**	**0.87 ± 0.00**	**126.09 ± 7.15**	**19.81 ± 0.66**	**0.83 ± 0.01**	**11.9 ± 0.1**	**05:02 ± 00:46**
Dataset 1 Baseline	268.03 ± 4.23	20.45 ± 0.27	0.84 ± 0.00	296.93 ± 4.83	21.74 ± 0.29	0.78 ± 0.00	36.4 ± 7.9	16:29 ± 03:35
Dataset 1 CSI2Image	392.46 ± 1.10	39.14 ± 1.94	0.58 ± 0.06	349.87 ± 15.87	45.57 ± 2.47	0.49 ± 0.04	67.8 ± 1.7	15:28 ± 5:09
Dataset 2 LatentCSI	**28.21 ± 0.78**	7.87 ± 0.09	0.94 ± 0.00	**27.90 ± 0.43**	7.90 ± 0.03	0.92 ± 0.00	**17.9 ± 0.2**	**16:24 ± 00:03**
Dataset 2 Baseline	47.67 ± 2.04	**7.15 ± 0.50**	**0.97 ± 0.00**	69.34 ± 2.50	**7.19 ± 0.24**	**0.93 ± 0.00**	59.3 ± 0.2	91:09 ± 19:19
Dataset 2 CSI2Image	312.24 ± 2.15	24.15 ± 0.64	0.76 ± 0.03	372.99 ± 10.25	49.72 ± 0.65	0.46 ± 0.02	73.0 ± 2.3	32:53 ± 10:09

TABLE IV
TEXT-GUIDED CSI IMAGE GENERATION

	Reference	"a photograph of a man in a small office room, 4k, realistic"	"a drawing of a man in a laboratory, anime, 4k"
Dataset 1	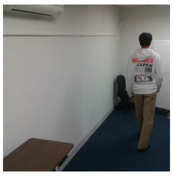	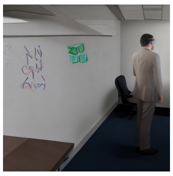	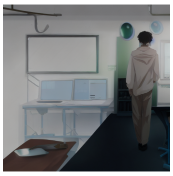
Dataset 2	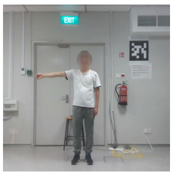	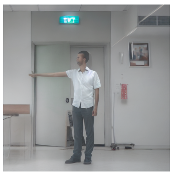	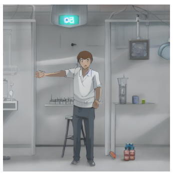

latent representations through natural language prompts. As illustrated in Table IV, LatentCSI can generate stylistic and semantic variations of an image from the same CSI input using different text prompts. For the results shown, we employ 100 denoising steps of DDIM [13] with a noise strength of 0.6 which determines the variance of noise added.

Due to the dimensionality bottleneck in LatentCSI, high-frequency details—such as facial features, fine textures, or text—are not preserved. Text-based conditioning allows us to reconstruct or augment these elements according to a specified prompt, enabling stylistic transformation and controlled editing of semantically relevant content.

IV. CONCLUSION

We presented LatentCSI, a novel approach for high-resolution image generation from CSI by leveraging the power of a pretrained latent diffusion model. Rather than generating images directly in pixel space—which is computationally expensive and often requires complex training procedures—we propose a framework that maps CSI amplitudes into the latent space of the LDM using a lightweight neural network. This design reduces computational load and simplifies training while improving perceptual quality compared to conventional end-to-end architectures, even when the end-to-end model achieves better pixel accuracy. The use of the LDM's latent space provides a natural process to harness the power of text-guided image editing using diffusion. This allows for fine-grained control over the output, which is particularly valuable in privacy-sensitive contexts. We suggest that LatentCSI is a compelling alternative to existing CSI-to-image methods, offering superior image quality, efficiency, and controllability.

REFERENCES

[1] Y. Ma, G. Zhou, and S. Wang, "WiFi Sensing with Channel State Information: A Survey," *ACM Comput. Surv.*, vol. 52, no. 3, 46:1–46:36, Jun. 2019.

[2] I. J. Goodfellow et al., "Generative Adversarial Nets," in *Advances in Neural Information Processing Systems*, vol. 27, Curran Associates, Inc., 2014.

[3] S. Kato et al., "CSI2Image: Image Reconstruction From Channel State Information Using Generative Adversarial Networks," *IEEE Access*, vol. 9, pp. 47 154–47 168, 2021.

[4] C. Yu et al., "WiFi-Based Human Pose Image Generation," in *2022 IEEE 24th International Workshop on Multimedia Signal Processing (MMSP)*, Sep. 2022, pp. 1–6.

[5] C. Yu, Z. Wu, D. Zhang, Z. Lu, Y. Hu, and Y. Chen, "RFGAN: RF-Based Human Synthesis," *IEEE Transactions on Multimedia*, vol. 25, pp. 2926–2938, 2023.

[6] M. Arjovsky and L. Bottou, "Towards Principled Methods for Training Generative Adversarial Networks," in *International Conference on Learning Representations*, Feb. 2017.

[7] J. Strohmayer, R. Sterzinger, C. Stippel, and M. Kampel, "Through-Wall Imaging Based On WiFi Channel State Information," in *2024 IEEE International Conference on Image Processing (ICIP)*, Oct. 2024, pp. 4000–4006.

[8] J. Yang et al., "MM-Fi: Multi-Modal Non-Intrusive 4D Human Dataset for Versatile Wireless Sensing," in *Thirty-Seventh Conference on Neural Information Processing Systems Datasets and Benchmarks Track*, Nov. 2023.

[9] R. Rombach, A. Blattmann, D. Lorenz, P. Esser, and B. Ommer, "High-Resolution Image Synthesis with Latent Diffusion Models," in *2022 IEEE/CVF Conference on Computer Vision and Pattern Recognition (CVPR)*, Jun. 2022, pp. 10 674–10 685.

[10] C. Meng et al., "SDEdit: Guided Image Synthesis and Editing with Stochastic Differential Equations," in *International Conference on Learning Representations*, Aug. 2021.

[11] J. Redmon and A. Farhadi, *YOLOv3: An Incremental Improvement*, Apr. 2018. arXiv: 1804.02767 [cs].

[12] M. Hutar, P. Brida, and J. Machaj. "FeitCSI, the 802.11 CSI tool."

[13] J. Song, C. Meng, and S. Ermon, "Denoising Diffusion Implicit Models," in *International Conference on Learning Representations*, Oct. 2020.